

Energy and Thermofluids Engineering



Available at https://asps-journals.com

Simulation and validation of phase change heat exchangers

- P. S. Arshi Banu¹, Md Azhar^{2⊠}, I.M. Mahbubul³, Gnana Sagaya Raj⁴
- 1 Department of Mechanical Engineering, Hindustan Institute of Technology & Science, Padur-603103, India
- 2 Department of Mechanical Engineering, Maulana Mukhtar Ahmad Nadvi Technical Campus, Malegaon-423203, Maharashtra, India
- 3 Institute of Energy Engineering, Dhaka University of Engineering & Technology, Gazipur (DUET), Gazipur-1707, Bangladesh
- 4 Department of Mechanical Engineering, Sree Vidyanikethan Engineering College, Tirupati 517102, India

Received May 12, 2023 Revised December 18, 2023 Accepted January 18, 2024

Published online: February 21, 2024

Keywords
Heat Exchanger
Condensation
Evaporation
CFD analysis

SIMULINK

Abstract: Due to the depletion of fossil fuel resources and environmental problems caused by global warming, energy generation has greater potential in future engineering. In designing of thermal or refrigeration system phase change heat exchangers play a vital role. Prior to the application of these realistic models, proper analysis is critical. It will provide accurate findings while also reducing research effort, risk, and expense. Analytically, we investigated condensation and evaporation in a fin-tube heat exchanger using ANSYS FLUENT 2022. The fluid flowing inside the tube is refrigerant R22 and the fin side external fluid is considered as atmospheric air. To understand its physical and mathematical behavior, the CFD findings have been validated with MATLAB Simulink. Variations of heat transfer coefficients and pressure drops of the air-side and refrigerant side with various geometry parameters such as tube diameter, fin spacing, and number of rows have been plotted and observed. Results show that the heat transfer coefficient varies from 77.4 W/m²K to 65.6 W/m²K on the air side while 8787 W/m²K to 6339 W/m²K on the Refrigeration tube side. Additionally, the pressure drop varies from 0.0265 kPa to 0.0353 kPa on the air side while 33.1 kPa to 26.2 kPa on the Refrigeration tube side.

© 2024 The authors. Published by Alwaha Scientific Publishing Services SARL, ASPS. This is an open access article under the CC BY license.

1. Introduction

Global warming causes the temperature of the surrounding air to rise every year (Gray, 2000). Staying inside without a good cooling system is not pleasant. Air conditioners are becoming a common household item around the world as a means of bringing indoor temperature into the human comfort zone (Azhar and Siddiqui, 2017). To remove heat from the room evaporation takes place in the indoor unit and rejection of heat i.e., condensation in the outdoor unit. Evaporation is the process of converting a liquid to a vapor by absorbing heat. Condensation is the process of converting a vapor to a

liquid by removing heat (Yunus and Ghajar, 2020). This process is carried through a heat exchanger (HE). Heat exchangers are devices that are usually used for heat transfer between two running fluids at unlike temperatures (Khairul et al., 2014). FT-type HEs are preferred in the case where low heat transfer coefficient on the outside of the tubes. Fin and tube heat exchangers (FT type HE) have long been popular in the refrigeration, aerospace, and other industrial sectors (Kraus, et al., 2001). FT type HE (FT-HE) has tubes with a larger outside surface area or fins, which helps to increase the heat transfer rate. The increased heat transfer area generated by the fins in these circumstances aids in ensuring that the required rate of heat transfer is

 $^{^{}oxdot{M}}$ Corresponding author. E-mail address: md_azhar@zhcet.ac.in

achieved. Working fluids for these applications have included a variety of chlorofluorocarbon (CFC) and hydrochlorofluorocarbon (HCFC) refrigerants. The use of CFC refrigerants has been prohibited due to major ozone layer depletion and global warming concerns (McCulloch et al., 2003), and the most widely used HCFC refrigerants are R-22, R-134a, R-143a, R-407c, R-410a, R-417a, and R-507 necessitating the study of their thermodynamic (Gopalnarayanan, 1998), thermophysical, and heat transfer properties (Xiang et al., 2014).

Here, a few of the fin and tube heat exchangers' literary works have been discussed. In an experimental assessment of the pressure drop and heat transfer during the condensation of the refrigerant R-134a in a HE having vertical plate configuration, (Djordjević et al., 2008) discovered that both variables rise with the quality of the rising vapor. The convective effect predominates the heat transfer at the refrigerant side, according to (Shi et al., 2010) experimental investigation of condensation heat transfer and pressure drop of R134a in a plate HE. They discovered that the high vapor quality zone and mass flux have a significant impact on condensation heat transfer using R1234ze(E) and R32 as refrigerants, (Luyben et al., 2019) conducted an experimental investigation on the evaporation heat transfer and two-phase characteristics of a vertical upward flow and discovered that R32 had a higher heat transfer coefficient than R1234ze(E), regardless of the mass flux and quality, particularly at lower mass flux conditions. The Open FOAM framework was used by Thomas (Kleiner et al., 2019) to design and implement a CFD solver for thermally induced pure material condensation. They discovered that the heat transfer coefficients are slightly lower than those predicted by Nusselt's film theory but are still in excellent agreement with the experimental data. To quantify the heat transfer coefficient for MED falling film evaporator application, (Tahir et al., 2021) created a two-dimensional (2D) CFD model. They discovered that the heat transfer coefficient is maximal at the impact zone and subsequently declines as the liquid travels around the tube. The heat transfer coefficient at Ti = 85°C is 43.5% greater than that at Ti = 5°C for a liquid load of 0.09 kg/(ms). To understand the Marangoni condensation phenomenon, (Park and Choi, 2020) conducted a CFD study for the condensation heat transfer of steam-ethanol mixtures on a horizontal tube. They discovered that as the ethanol vapor concentration increased from 0% to 0.1%, the heat flux of the vapor

mixture became 1.2 times greater. Hu et al. (Hu et al., 2017) investigated the ethanol-water vapor in a commercial plate HE to find out the Local heat transfer coefficient considering the Marangoni effect. Using an ANSYS Fluent, (Mohammed et al., 2019) simulated the evaporation and condensation of acetone in a horizontal tube and discovered that the phase change rate increases when the velocity lowers and the wall temperature rises (evaporation case) or falls (condensation case).

It is observed from open literature that a comparison of simulation of condensation and evaporation in an FT-HE under MATLAB SIMULINK and ANSYS is missing. Therefore, the goal of the present study is to design and evaluate a phase change HE with R22 as refrigerant and air as an external fluid. To investigate how the geometrical parameters of the condensation and evaporation phases of a HE affects the behavior of heat transfer coefficients. contrasting the outcomes of the two pieces of work using similar input parameters and experimental outcomes. Assessing the advantages and disadvantages of each method.

Also, there are two types of thermodynamic analysis of vapor absorption refrigeration systems (Arshi Banu et al., 2023). One is the first law analysis and the other one is the second law analysis or exergy analysis. In the first law analysis performance or COP enhancement is possible by changing the number of cascading effects, and thermophysical properties of the refrigerant-absorbent combination. There is no direct impact on component design or selection in this analysis. Second law analysis (Arshi Banu et al., 2020) provides availability losses of each component of the system such as the absorber, generator, condenser, and evaporator. All these components are HE where heat transfer and phase change take place. In the Generator and absorber mass transfer also takes place. In the experimental work on absorbers (Banu et al., 2022), it was observed that the design of the phase change heat exchanging component is very important. It plays a major role in the overall performance of the refrigeration system. Hence, numerical investigations of the HEs (Arshi Banu et al., 2022a, 2022b) show the heat transfer coefficient's behavior concerning flow rates of hot and cold fluids and their temperatures. The design-based analysis such as the influence of geometric parameters on phase change HEs have been investigated in the present work.

2. Design Specifications

Table 1 shows the specifications of the FT-type heat exchanger. Copper-tubed heat exchangers are the tubes that were taken into consideration for the current task. R22, which is going through the tube, is the fluid that is accounted for Fig. 1 depicts the heat exchanger that was used for the analysis.

3. CFD Analysis

Computational fluid dynamics (CFD) is used in ANSYS Fluent to model fluid flow and heat transfer problems. A range of fluid processes, including fluid-structure multiphysics interactions, are modeled and simulated using this CFD program. In the case of industrial applications, heat transfer, turbulence, and reactions are also considered along with fluid flow. It comes with a complete collection of tools for physical modeling (Luyben, 2014).

Table 1. Specifications of FT type HE.

Parameter	Condenser	Evaporator
Pitch of tubes Horizontal, P1 X Vertical, P2 [mm]	25 X 25	25 X 25
Pitch of tubes on the diagonal plane in staggering arrays, P ₃ , [mm]	27	27
Length of tube, L _t , [mm]	291	291
Fin outer diameter, D _t , [mm]	10 (8 to 13)	10.0
Height of the fin, L= $(c-D_t)/2$, [mm]	4	4
Width of the fin, b _f , [cm]	91.4	n/a
Fin length, I _f , [cm]	76.2	45.7
Fin thickness, w, [mm]	82.6	63.5
Space in two consecutive fins, s, [mm]	3 (3 to 5.5)	3
Total No. of rows, n _r	2(2 to 4)	2
Tubes number in single row, n _t	8	8
Number of tubes, N= n _t x n _r	16	16

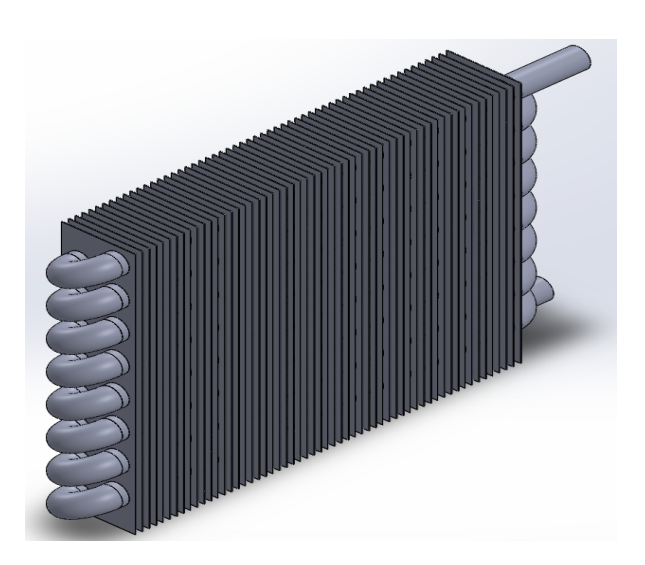


Fig.1 CAD model of phase change Fin-Tube Heat Exchanger.

3.1. Design of Heat Exchanger

According to ANSYS Space claim, the heat exchanger is developed. There are primarily four sections of the heat exchanger under consideration for study.

- Fluid domain
- Air Domain
- Fins
- Tubes

Using the EXTRUDE command, a circle with a diameter of 10 mm was extruded through the midplane up to 291 mm and saved as a single component. By selecting the top plane, a second circle with a diameter of 8 mm has been formed. Semi-arc and circle have been linked under the command of SWEEP. The rectangle is sketched and extruded through 5 mm, measuring 115 mm in width and 380 mm in length. On the front face of the fin, two circles with a diameter of 10 mm have been drawn. A linear pattern with a length of 25 mm and 12 numbers has been chosen, and the cut has been extruded through the fin. The fin and tube heat exchanger's 3D model is created once all the individual components have been put together. The control volume has been established and the ENCLOSER command has been chosen. Using the BOOLEAN command, the tube, fins, and fluid domain have been removed from the enclosure.

3.2 Meshing of FT type HE

Ansys 2021 R1 is the software used to mesh the data [9]. The skewness should be less than 0.94 and the elements kept should be fewer than five lakhs as this is the student version. For greater design quality, less skewness in the meshing must be maintained. Following is how meshing is carried out:

- The geometry in Fig. 1 has been meshed using the patch tetrahedral approach.
- The tube's body size was determined to be 8mm.
- The body size that was taken into account for the fluid domain was 4.5mm.
- The enclosure's body size consideration is 6mm.
- A 5mm body size is taken into account for the fins.
- The skewness was determined to be 0.81.
- A total of 412208 elements were retrieved.
- The following contact regions have been chosen based on the design.

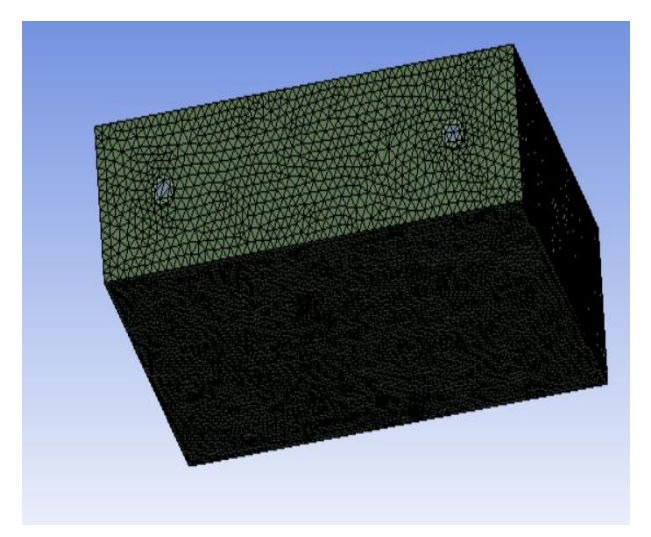


Fig.2 Heat exchanger meshing

- The tube as a fluid domain
- Air domain for both tubes and fins
- Fluid domain faces have been chosen, and their names are based on the flow direction.

The meshing has been changed to match the aforementioned modifications seen in Fig 2.

3.3 Setup

- In the first step of the simulation, the energy and viscous models have been selected. Under the viscous model, improved wall treatment options were selected and a Multiphase of VOF has also been selected.
- Air and R22 have been selected as working fluids.
 Copper (Cu) and aluminum (Al) as a solid material have been used for both condensation and evaporation.
- The primary phase for evaporation is liquid and the secondary phase is gas.
- R22 is considered a hot fluid, while air is a cold fluid.
 For cell zone conditions. Al has been selected for both the fins however Cu has been adopted for the inner tube.
- R22 side boundary conditions are given.
- Air side boundary conditions are also given as shown in Fig 3.
- To detect missing contact regions, Mesh interfaces have been verified.
- For the solution, the Second order has been selected.
- Hybrid initialization provided.
- 500 iterations have been taken to run the problem.
- After completing these steps, the results are obtained that have been discussed in the coming section.

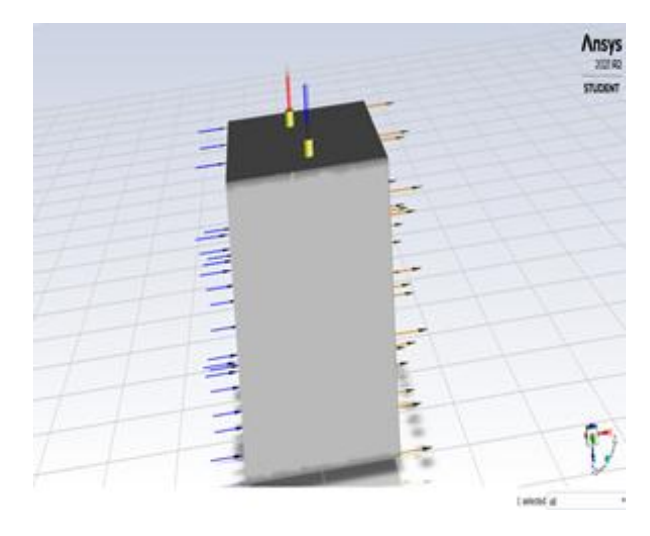


Fig.3 Inlet and outlet of external air domain of Heat exchanger

4. Simulation Using MATLAB Simulink

4.1 Refrigerant side heat transfer coefficient

A mass flow rate of refrigerant (m)

 $Q=m \times h_{fa}$

$$m = \frac{Q}{h_{fg}} \tag{1}$$

Velocity of refrigerant (v)

 $m=\rho Av$

$$v = \frac{\rho \times A}{m} \tag{2}$$

Reynold's Number
$$Re = \frac{V * D * \rho}{\mu}$$
 (3)

Heat transfer coefficient of liquid side (h_L)

 $Nu=0.028*Re^{0.8}*pr^{0.3}$

$$h_L = \frac{Nu * k}{D} \frac{W}{m^2 K} \tag{4}$$

The condensation heat transfer coefficient of the condenser (h_c)

$$h_C = h_L(0.55 + \frac{2.09}{P_T^{0.38}}) \tag{5}$$

Pressure drop due to friction in pipe
$$\Delta p = \frac{fG^2L}{\rho}$$
 (6)

f = friction factor

Momentum pressure drop(Δp_t)= $\frac{G^2}{\rho_v g_c} \left\{ \left[1 + \left(\frac{\rho_v}{\rho_l} \right) - \right] \right\}$

$$\left(\frac{\rho_{v}}{\rho_{l}}\right)^{1/3} - \left(\frac{\rho_{v}}{\rho_{l}}\right)^{2/3} x^{2} - \left[2\left(\frac{\rho_{v}}{\rho_{l}}\right) - \left(\frac{\rho_{v}}{\rho_{l}}\right)^{1/3} - \left(\frac{\rho_{v}}{\rho_{l}}\right)^{2/3}\right] x$$
(7)

The total tube inside pressure $\Delta p = \Delta p_f + \Delta p_t$

Heat transfer coefficient of evaporation (he)

$$\begin{split} h_e &= (0.0186875) \frac{\kappa_l}{D^{0.2}} \left(\frac{G}{\mu_l}\right)^{0.8} \left(\frac{\mu_l * C p_l}{\kappa_l}\right)^{0.4} \left(\frac{\rho_l}{\rho_v}\right)^{0.375} \left(\frac{\mu_v}{\mu_l}\right)^{0.075} \\ \left(\frac{\kappa_e - \kappa_l}{\kappa_a^{0.325} - \chi_l^{0.325}}\right) \end{split} \tag{9}$$

D = tube diameter G = mass flux k = conductivity ()_I = properties evaluated at saturated liquid stage ()_v = properties evaluated at saturated vapor stage ()_e = properties evaluated at exit ()_i = properties evaluated at inlet

4.2 Air side heat transfer coefficient

Surface area of fins

$$A_f = 2(c^2 - 0.785(D_t^2) + 2cw) \frac{Nl_t}{(s+w)}$$
 (10)

The surface area of the tubes (between two fins)

$$A_w = \frac{Nl_t}{(s+w)} (D_t s) \tag{11}$$

Finned tubes' total surface area:

$$A=A_f + A_w \tag{12}$$

Total tube surface area (without fins removed)

$$A_t = NL_t \pi D_t \tag{13}$$

Minimum cross-section area

$$S_{min} = n_t l_t (P_1 - D_t - \frac{2wL}{(s+w)})$$
 (14)

$$V_{max} = \frac{m_a}{S_{min}\rho} \tag{15}$$

Reynold's number
$$Re = \frac{V_{max} \rho D_t}{u}$$
 (16)

4.3 Average heat transfer coefficient (for low fin tubes)

Nu= 0.183Re^{0.7}
$$(\frac{S}{L})^{0.36} (\frac{P_1}{D_t})^{0.06} (\frac{L}{D_t})^{0.11} Pr^{0.36} F_1 F_2 F_3$$
 (17)

 F_1 = fluid property variation factor.

 F_2 = number of tube rows factor.

 F_3 = Factor for tube arrangement.

$$h = \frac{Nu \, k}{D_t} \tag{18}$$

4.4. Fin efficiency

$$\eta_f = \frac{tanhm\psi}{m\psi} \tag{19}$$

$$\psi = \frac{D_t}{2} \left(\frac{c}{D_t} - 1 \right) \left(1 + 0.35 \ln \frac{c}{D_t} \right) \tag{20}$$

$$m = \sqrt{\frac{hP}{KA}} \tag{21}$$

4.5 The effective average heat transfer coefficient (H)

$$ho = \left(\frac{\eta_f A_t + A_w}{A}\right) h \tag{22}$$

Pressure drop due to fins $\Delta p_f = f_f v_m \frac{G_{max}^2 A_f}{2}$

where: f_f = fin friction factor v_m = mean specific volume G_{max} = mass velocity through minimum area A_f = fin surface area A_c = minimum free-flow cross sectional area

Pressure drop due to bank of tubes $\Delta p_{tube} = Eu_c \frac{G_{max}^2}{2\rho} z$

 Eu_c = corrected Euler number

z = number of rows

Total air side pressure $\Delta p = \Delta p_f + \Delta p_t$

The Fig. 4 illustrates Simulink's tools. Which has four major command like 'input', 'subsystem', 'goto', and 'display'.

5. Results and discussions

After performing the geometry, meshing and setup operations of the phase change heat exchangers in ANSYS Fluent, the result obtained from CFD analysis are discussed in this section. Figure 5 shows the volume fraction variation of refrigerant in the evaporator. In this Figure the value 'zero' represent saturated liquid form and 'one' represent saturated vapour form. The evaporation in the evaporator can be seen with the volume fraction variations. Figure 6. depicts the volume fraction variation of refrigerant in the

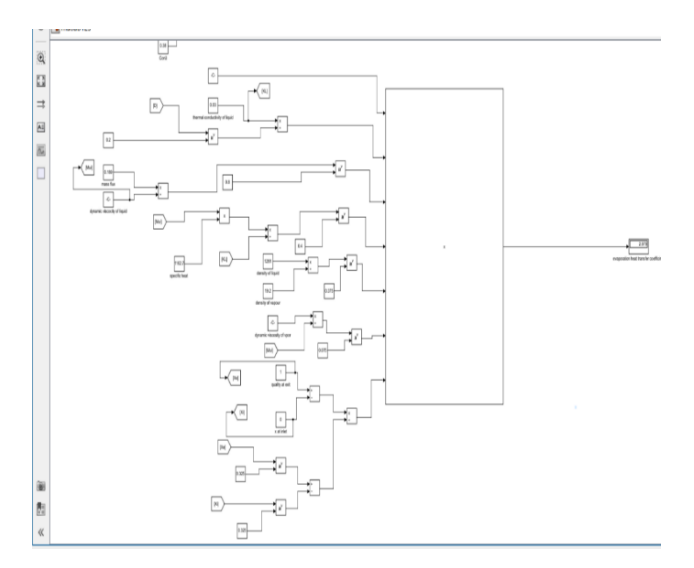


Fig. 4. Simulation model of Heat exchanger in MATLAB Simulink.

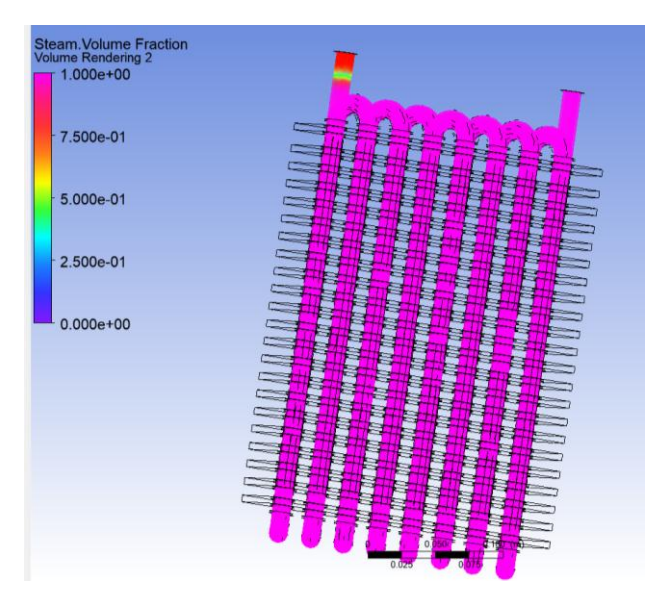


Fig. 5 Evaporation volume fraction profile

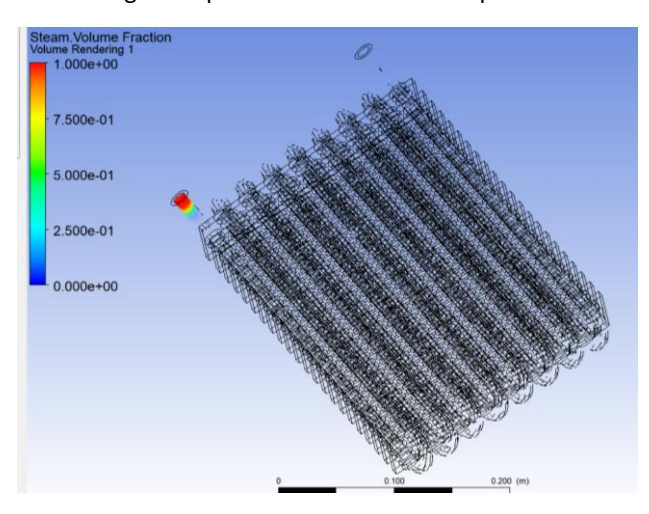


Fig. 6 Condenser volume fraction profile.

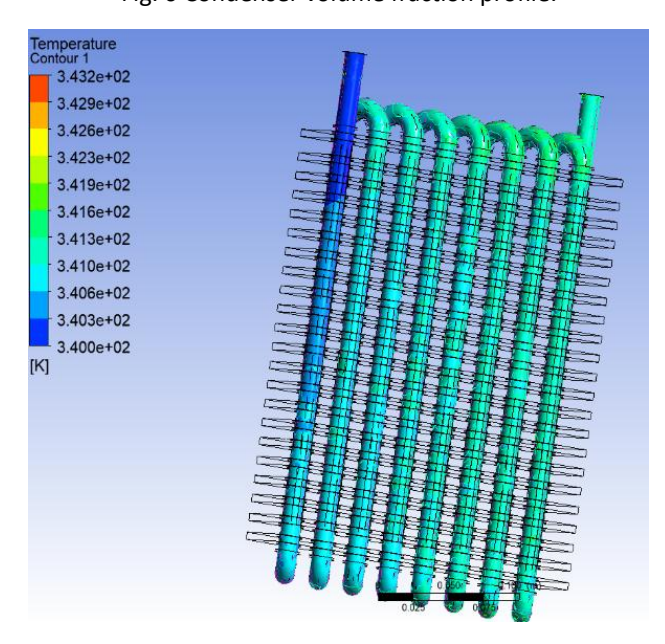


Fig. 7 Condenser temperature profile.

condenser. Again, in this Figure, the value 'one' represents saturated vapor form, and 'zero' represents saturated liquid form. The condensation in the condenser can be seen with the volume fraction variations. Figure 7 represents the temperature variation in the condenser tubes during condensation.

The results obtained from Simulink are discussed in Figure 8. The first geometric parameter considered is the diameter of the tube. The plots of Figure 8 show the variation of the air-side heat transfer coefficient and refrigeration-side heat transfer coefficient with the tube diameter of the condenser. Three tube diameters of 7.94 mm, 9.53 mm, and 12.7 mm were considered. By keeping the fin pitch at 4.72 per cm with two rows and frontal area constant. It has been observed that the heat transfer coefficient is decreasing concerning diameter. The air-side heat transfer coefficient varies from 77.4 W/m²K to 65.6 W/m²K. Refrigeration tube side heat transfer coefficient varying from 8787 W/m²K to 6339 W/m²K. It is known that the heat transfer coefficient is inversely proportional to the diameter of the tubes.

The plots of Figure 9 show the variation of air-side pressure drop and refrigeration tube side pressure drop with the tube diameter of the condenser. The same tube diameters of 7.94 mm, 9.53 mm, and 12.7 mm were considered. By keeping the fin pitch at 4.72 per cm with two rows and frontal area constant. Airside pressure drop varies from 0.0265 kPa to 0.0353 kPa. Refrigeration tube side pressure drop varying from 33.1 kPa to 26.2 kPa. It has been observed that the air side pressure drop is increasing and the refrigeration tube side pressure drop is decreasing with an increase in tube diameter. Hence 11.3 mm diameter is considered as optimum diameter where both the pressures drop and heat transfer coefficients of the air side and refrigerant tube side.

The second geometric parameter considered in Figure 10 is the fin pitch. It shows the variation of air-side heat transfer coefficient and refrigeration tube-side heat transfer coefficient with fin pitch. Fin pitch varies from 3.15, 3.94, 4.72, and 5.51 per cm, by keeping tube diameter at 12.7 mm and frontal area constant. It is observed that both heat transfer coefficients (air side and tube side) are decreasing with fin pitch. The air-side heat transfer coefficient varies from 66.9 W/m²K to 61 W/m²K. Refrigeration tube side heat transfer coefficient varying from 6408 W/m²K to 6329 W/m²K.

Figure 11 is the variation of the same pitch dimensions as in Figure 9 with air side and refrigeration tube side pressure drop. It is observed that the air side pressure drop varies from 0.037 kPa to 0.054 kPa and the refrigeration tube side pressure drop varies from 44.1 kPa to 34.5 kPa with the increase in fin pitch. It has been observed that the air side

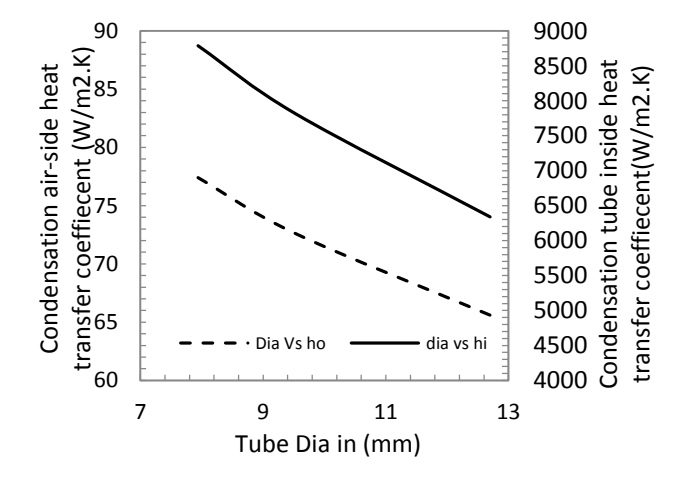


Fig.8 Condensation heat transfer coefficient vs Diameter of tube

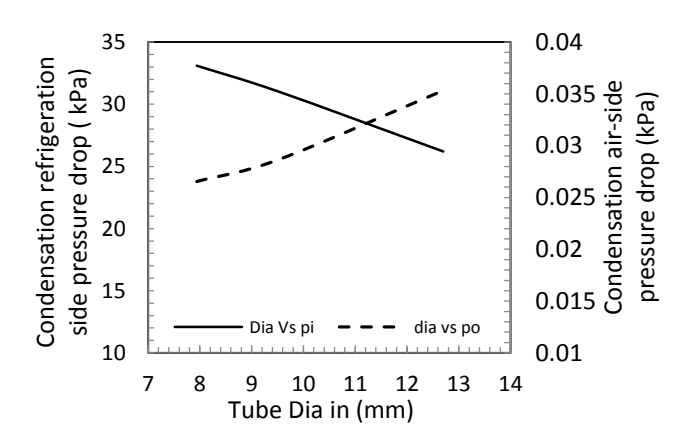


Fig. 9 Condenser pressure drop vs Diameter of tube.

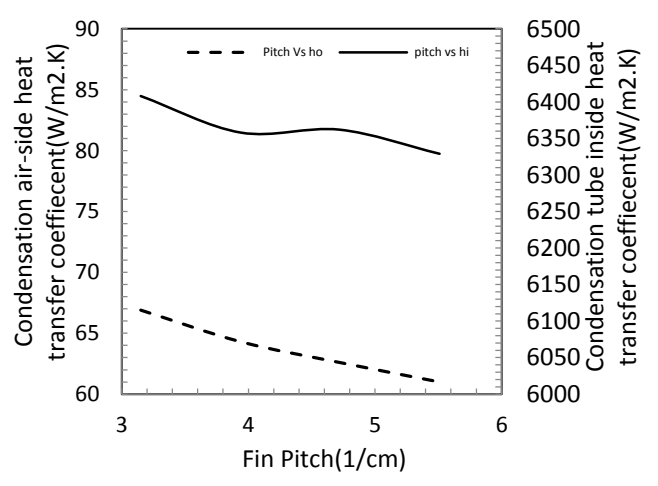


Fig. 10 Condensation heat transfer coefficient vs Fin Pitch.

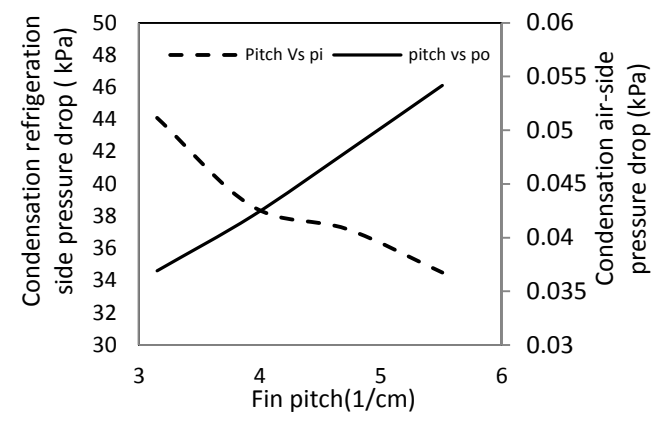


Fig. 11 Condenser pressure drop vs fin pitch.

pressure drop is increasing and the refrigeration tube side pressure drop is decreasing with an increase in fin pitch. Hence it inferred that 4 1/cm pitch is considered as the optimum pitch where both the pressures drop and heat transfer coefficients of airside and refrigerant tube side

The third geometric parameter considered in Figure 12 is the number of rows of tubes. It shows the variation of air-side heat transfer coefficient and refrigeration tube side heat transfer coefficient with the number of rows. The number of rows varied to 2, 3, and 4, by keeping the tube diameter at 12.7 mm, fin pitch 4.72/cm, and frontal area as constant. It is observed that both heat transfer coefficients (air side and tube side) are decreasing with an increase in number of rows. The air-side heat transfer coefficient is varying from 65.6 W/m²K to 52.6 W/m²K. Refrigeration tube side heat transfer coefficient varying from 6339 W/m²K to 4675 W/m²K.

Figure 13 is the variation of the same number of rows as in Figure 9 with air side and refrigeration tube side pressure drop. It is observed that the air side pressure drop varies from 0.035 kPa to 0.042 kPa and the refrigeration tube side

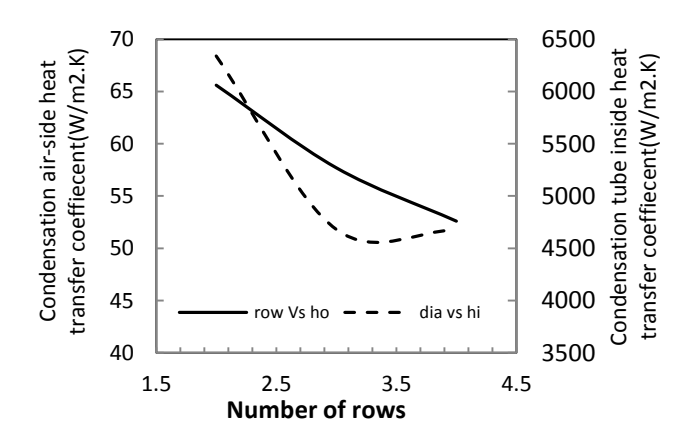


Fig. 12 Condensation heat transfer coefficient vs No. of rows of tube

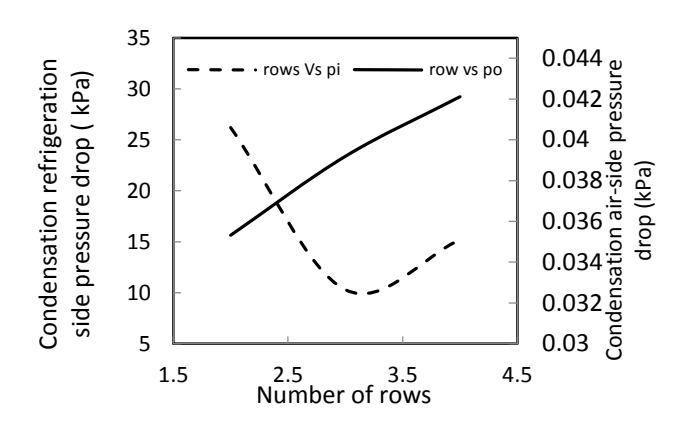


Fig. 13 Condenser pressure drop vs Number of rows

Pressure drop varies from 26.2 kPa to 15.2 kPa with the increase in fin pitch. It has been observed that the air side pressure drop is increasing and the refrigeration tube side pressure drop is decreasing with an increase in fin pitch. Hence it inferred that the least number of rows are better for both optimum pressure drop and heat transfer coefficients of the air side and refrigerant tube side.

6. Conclusion

- For phase change Fin and tube-type Heat Exchanger simulation has been done with MATLAB Simulink.
- Variations of heat transfer coefficient and pressure drop of Heat Exchanger with geometric parameters such as tube diameter, fin pitch, and the number of tubes have been presented.
- Optimum geometric parametric values have been identified.
- CFD analysis has been carried out for the same model for validation and comparison.
- Volume fraction profiles have been discussed for both evaporation and condensation analysis.
- Heat transfer coefficient varies from 77.4 W/m²K to 65.6 W/m²K on the air side while 8787 W/m²K to 6339 W/m²K on the Refrigeration tube side.
- Pressure drop varies from 0.0265 kPa to 0.0353 kPa on the air side while 33.1 kPa to 26.2 kPa on the Refrigeration tube side.
- Finally, it is inferred from the present study that the least number of rows is better for both optimum pressure-drop and heat-transfer coefficients of the airside and refrigerant tube side.

Nomenclature

A Area

A_f Surface area of fins

A_t Total tube surface area (without fins removed)

A_w Surface area of the tubes (between two fins)

Ac minimum free-flow cross-sectional area

Af fin surface area

bf Width of the fin, mm

Cp Specific Heat

D tube diameter

Dt Fin outer diameter, mm

Euc corrected Euler number

f Friction factor

ff fin friction factor

G mass flux

Gmax mass velocity through minimum area

h_C Condensation heat transfer coefficient of condenser

he Heat transfer coefficient of evaporation

h_L Heat transfer coefficient of liquid side

ho (or) H The effective average heat transfer coefficient (air/fin side)

k conductivity

L Height of the fin, mm

If Fin length, mm

Lt Length of tube, mm

m Mass flow rate of refrigerant

m a Mass flow rate of air

N Number of tubes

nr Total No. of rows

nt Tubes number in a single row

P₁ Pitch of tubes in a plane perpendicular to the flow, mm

P₂ Pitch of tubes in direction of flow, mm

P₃ Pitch of tubes on the diagonal plane in staggering arrays, mm

s Space in two consecutive fins, mm

S min Minimum cross-section area

v Velocity of refrigerant

V_max Maximum air velocity

vm mean specific volume

w Fin thickness, mm

x quality

z number of rows

η_f Fin efficiency

μ viscosity

ρ density

ψ Fin parameter

()e properties evaluated at exit

()i properties evaluated at inlet

()I properties evaluated at saturated liquid stage

()v properties evaluated at saturated vapor stage

Δp Total pressure

Δp Pressure drop due to friction in pipe

Δp_f Pressure drop due to fins

Δp_t Momentum pressure drop

 Δp_{tube} Pressure drop due to bank of tubes

Disclosures

Free Access to this article is sponsored by SARL ALPHA CRISTO INDUSTRIAL.

References

- ANSYS Student version Available on: https://www.ansys.com/enin/academic/students/ansys-student
- Arshi Banu, P.S., Dhanapal, B., Mathevan Pillai, T., Chellappa, B., Sathyamurthy, R., 2022a. Thermodynamic and hydraulic design characteristics of the fin tube heat exchanger. Mater. Today Proc. 62, 2380–2387.
 - https://doi.org/10.1016/j.matpr.2022.04.853
- Arshi Banu, P.S., Mahbubul, I.M., Azhar, M., 2023. Chapter 2 Solar-operated vapor absorption cooling system, in: Jeguirim, M., Dutournié, P.B.T.-R.E.P. and D. (Eds.), Advances in Renewable Energy Technologies. Academic Press, pp. 63–107. https://doi.org/10.1016/B978-0-443-18439-0.00012-4
- Arshi Banu, P.S., Micha Premkumar, T., Sivamani, S., Vijayabalan, P., 2020. A detailed second law (excergic) analysis approach of H2O-LiBr vapour absorption cooling system. IOP Conf. Ser. Mater. Sci. Eng. 998, 12062.
 - https://doi.org/10.1088/1757-899X/998/1/012062
- Arshi Banu, P.S., N. S. Ramesh Lohith, D., Praveen Kalyan, M., Vempati, D.S., Hemanth Sai, B., 2022b. Simulation of fin and tube heat exchanger and validation with CFD analysis. Mater. Today Proc. 66, 1471–1476. https://doi.org/10.1016/j.matpr.2022.05.552
- Azhar, M., Siddiqui, M.A., 2017. Optimization of operating temperatures in the gas operated single to triple effect vapour absorption refrigeration cycles. Int. J. Refrig. 82, 401–425. https://doi.org/10.1016/j.ijrefrig.2017.06.033
- Banu, P.S.A., Lohith, D.N.S.R., Kalyan, M.P., Sai, V.D., Sai,B.H., 2022. Simulation of double pipe heat exchangerand validation with CFD analysis. AIP Conf. Proc.

2648, 40004. https://doi.org/10.1063/5.0116411

Djordjević, E.M., Kabelac, S., Šerbanović, S.P., 2008. Heat transfer coefficient and pressure drop during refrigerant R-134a condensation in a plate heat

- exchanger. Chem. Pap. 62, 78–85. https://doi.org/10.2478/s11696-007-0082-8
- Gopalnarayanan, S., 1998. Choosing the Right Refrigerant. Mech. Eng. 120, 92–95. https://doi.org/10.1115/1.1998-OCT-6
- Gray, V., 2000. The Cause of Global Warming. Energy Environ. 11, 613–629. https://doi.org/10.1260/0958305001500428
- Hu, S., Ma, X., Zhou, W., 2017. Condensation heat transfer of ethanol-water vapor in a plate heat exchanger.
 Appl. Therm. Eng. 113, 1047–1055.
 https://doi.org/10.1016/j.applthermaleng.2016.11.01
 3
- Khairul, M.A., Alim, M.A., Mahbubul, I.M., Saidur, R., Hepbasli, A., Hossain, A., 2014. Heat transfer performance and exergy analyses of a corrugated plate heat exchanger using metal oxide nanofluids. Int. Commun. Heat Mass Transf. 50, 8–14. https://doi.org/10.1016/j.icheatmasstransfer.2013.1 1.006
- Kleiner, T., Rehfeldt, S., Klein, H., 2019. CFD model and simulation of pure substance condensation on horizontal tubes using the volume of fluid method. Int. J. Heat Mass Transf. 138, 420–431. https://doi.org/10.1016/j.ijheatmasstransfer.2019.04.054
- Kraus, A., Aziz, A., Welty, J., Sekulic, D., 2001. Extended Surface Heat Transfer. Appl. Mech. Rev. 54, B92–B92. https://doi.org/10.1115/1.1399680
- Luyben, W.L., 2014. Heat exchanger simulations involving phase changes. Comput. Chem. Eng. 67, 133–136. https://doi.org/10.1016/j.compchemeng.2014.04.00 2
- Luyben, W.L., Yan, Y.-Y., Lin, T.-F., Mohammed, H.I., Giddings, D., Walker, G.S., Park, H.C., Choi, H.S., Tahir, F., Mabrouk, A., Koç, M., Kleiner, T., Rehfeldt, S., Klein, H., Jige, D., Sugihara, K., Inoue, N., 2019. Evaporation heat transfer and flow characteristics of vertical upward flow in a plate-fin heat exchanger. Int. J. Heat Mass Transf. 41, 4183–4194. https://doi.org/10.1016/S0017-9310(98)00127-6
 - https://doi.org/10.1016/S0017-9310(98)00127-6
- MATLAB Simulink Available on:https://www.Mathworks. com/academia /tahportal /hindustan -institute-oftechnology-and-science-31239439.h

- McCulloch, A., Midgley, P.M., Ashford, P., 2003. Releases of refrigerant gases (CFC-12, HCFC-22 and HFC-134a) to the atmosphere. Atmos. Environ. 37, 889–902. https://doi.org/10.1016/S1352-2310(02)00975-5
- Mohammed, H.I., Giddings, D., Walker, G.S., 2019. CFD multiphase modelling of the acetone condensation and evaporation process in a horizontal circular tube. Int. J. Heat Mass Transf. 134, 1159–1170. https://doi.org/10.1016/j.ijheatmasstransfer.2019.02 .062
- Park, H.C., Choi, H.S., 2020. CFD study of Marangoni condensation heat transfer of vapor mixture on a horizontal tube. Heat Mass Transf. 56, 2743–2755. https://doi.org/10.1007/s00231-020-02872-3
- Shi, Z.-Y., Chen, J.-P., Grabenstein, V., Kabelac, S., 2010. Experimental investigation on condensation heat transfer and pressure drop of R134a in a plate heat

- exchanger. Heat Mass Transf. 46, 1177–1185. https://doi.org/10.1007/s00231-010-0699-y
- Tahir, F., Mabrouk, A., Koç, M., 2021. Heat Transfer Coefficient Estimation of Falling Film for Horizontal Tube Multi-Effect Desalination Evaporator Using CFD. Int. J. Thermofluids 11, 100101. https://doi.org/10.1016/j.ijft.2021.100101
- Xiang, B., Patra, P.K., Montzka, S.A., Miller, S.M., Elkins, J.W., Moore, F.L., Atlas, E.L., Miller, B.R., Weiss, R.F., Prinn, R.G., Wofsy, S.C., 2014. Global emissions of refrigerants HCFC-22 and HFC-134a: Unforeseen seasonal contributions. Proc. Natl. Acad. Sci. 111, 17379–17384.
- Yunus, C., Ghajar, A., 2020. Heat and mass: fundamentals and applications, 5th ed. ed. McGraw-Hill

https://doi.org/10.1073/pnas.1417372111

Professional., New York,.